Available online at www.sciencedirect.com
SCIENCE DIRECT®
International Journal of Solids and Structures 43 (2006) 5132–5146
INTERNATIONAL JOURNAL OF SOLIDS and STRUCTURES
www.elsevier.com/locate/ijsolstr

Nonlinear energy-based relations and numerical procedure for multiaxial local analysis

G.M. Owolabi *, M.N.K. Singh

Department of Mechanical and Manufacturing Engineering, University of Manitoba, Winnipeg, Manitoba, Canada R3T 2N2

Received 17 April 2005; received in revised form 17 June 2005
Available online 15 August 2005

Abstract

In this paper, two sets of nonlinear energy-based approximate models are formulated and used to predict the local parameters in a two-phase composite system. A numerical procedure using Newton–Raphson method is developed to solve each system of nonlinear equations in small time steps. The procedure allows the estimation of the local parameters through various loading and unloading steps and therefore, is independent of a yield criterion. The local strain results obtained using the procedure are compared with experimental results obtained at the depth of circumferentially notched particulate metal matrix composite subjected to variable amplitude loads. The numerical results are in good agreement with corresponding experimental results for the geometry and load paths considered.

Keywords: Nonlinear relations; Equivalent strain energy density (ESED); Neuber's method; Variable amplitude loads; Composite system

1. Introduction

The development of robust analytical methods for estimating local parameters is an important step in fatigue life prediction in engineering components with material and/or geometric discontinuities. To make fatigue life prediction methods more conducive to average design environments, great research efforts have been directed to the development of simplified analytical techniques that are more computationally efficient. For multiaxial non-proportional loading, some of the existing models attempt to either incorporate the effect of geometric discontinuity into the constitutive relations, as in Barkey (1993), Barkey et al. (1994),

* Corresponding author. Tel.: +1 204 474 9173; fax: +1 204 275 7507.
E-mail address: gowolabi@yahoo.com (G.M. Owolabi).

0020-7683/$ - see front matter © 2005 Elsevier Ltd. All rights reserved.
doi:10.1016/j.ijsolstr.2005.06.051

Lee et al. (1995), and Gu and Lee (1997), or reformulate uniaxial approximation methods in incremental forms, as in Singh et al. (1996). However, it should be noted that the majority of the aforementioned efforts have been directed to monolithic materials. For heterogeneous materials such as particulate metal matrix composites (PMMCs), the authors developed some relations for predicting the inelastic behavior of PMMC components under monotonic loading (Owolabi and Singh, 2003a) and cyclic loading (Owolabi and Singh, 2005).

In this paper, two set of nonlinear energy-based relations are presented that can independently predict the local parameters for a two-phase composite system under complex variable amplitude loads. Newton–Raphson's method for solving a system of nonlinear equation is employed to develop a numerical solution procedure and is designed in a way that allows changing the form of the nonlinear approximate relations. Each model incorporates the material constitutive relations that define the material stress–strain relations and nonlinear approximate relations that relate the local parameters. Sections 2 and 3 present the constitutive relations and the nonlinear energy relations, respectively. The numerical procedure is discussed in Section 4. Section 5 presents the results, and Section 6 gives the conclusions.

2. Constitutive relations

For multiaxial cyclic loading, Owolabi and Singh (2003b) have developed constitutive relations, using the endochronic theory of plasticity (Valanis, 1980) and the incremental mean field theory (Li and Chen, 1990), to predict the constituents and the composite elastic–plastic strain and stress increments. The matrix constitutive relation is given as (Owolabi and Singh, 2003b)

$$\begin{aligned}\Delta\varepsilon_{ij(m)} = {} & \frac{1+\upsilon_m}{E_m}[\Delta\sigma_{ij} - V_f C_{klst(m)}(\mathbf{S}_{klst} - \mathbf{I}_{klst})L^{-1}(C_{klst(f)} - C_{klst(m)})C^{-1}_{klst(m)}\Delta\sigma_{ij}] \\ & - \frac{\upsilon_m}{E_{(m)}}[\Delta\sigma_{kk} - V_f C_{ilst(m)}(\mathbf{S}_{ilst} - \mathbf{I}_{ilst})L^{-1}(C_{ilst(f)} - C_{ilst(m)})C^{-1}_{ilst(m)}\Delta\sigma_{kk}]\delta_{ij} \\ & + \frac{\frac{1}{2}\left[(\Delta S_{ij(m)})_q + \sum_{r=1}^{r}(S^r_{ij(m)})_{q-1}(1-\mathrm{e}^{-\alpha_r\Delta z})\right]\Delta z}{\left[\sum_{r=1}^{r} C_r \frac{(1-\mathrm{e}^{-\alpha_r\Delta z})}{\alpha_r}\right]},\end{aligned} \tag{1}$$

where

$$\mathbf{L} = [(V_f - 1)\mathbf{C}_{(m)}(\mathbf{I} - \mathbf{S})] + \mathbf{C}_{(f)}[V_f(\mathbf{S} - \mathbf{I}) - \mathbf{S}] \tag{2}$$

and

$$(S^r_{ij(m)})_q = (S^r_{ij(m)})_{q-1}\mathrm{e}^{-\alpha_r\Delta z} + 2\frac{C_r}{\alpha_r}\frac{\Delta\varepsilon^p_{ij(m)}}{\Delta z}(1-\mathrm{e}^{-\alpha_r\Delta z}). \tag{3}$$

In Eqs. (1)–(3), $\Delta\varepsilon_{ij}$ and $\Delta\sigma_{ij}$ are increments in strain and stress tensors, respectively. V_f is the reinforcement (f) volume fraction. $\upsilon_{(m)}$ and $E_{(m)}$ are the matrix (m) Poisson's ratio and elastic modulus, respectively. C_m and C_f are the matrix and reinforcement stiffness matrices, respectively. C_r and α_r are material constants determined from the matrix uniaxial stress–strain curve (note that r is the order of a Dirichlet series described in Hsu et al., 1991; Owolabi and Singh, 2003b). ΔS and Δz are the increments in the deviatoric stress (S) tensor and intrinsic time scale (z) respectively. The intrinsic time scale is a measure of the plastic deformation in the material. $\mathbf{I}$ and $\mathbf{S}$ are the identity matrix and Eshelby's tensor, respectively. Subscripts i, j, k, l, s, and t are indices and q is the current loading step. Writing Eq. (1) fully on the notch tip elements of a circumferentially notched bar shown in Fig. 1(a), using three terms in the Dirichlet series, gives the following relations:

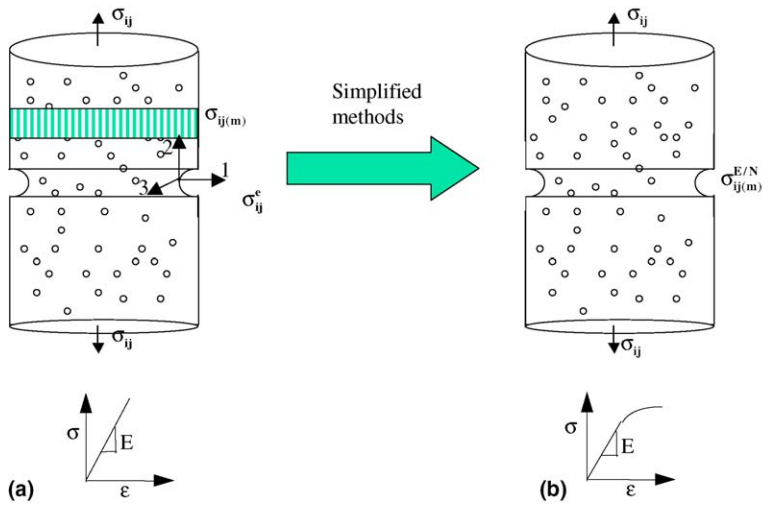

Fig. 1. Illustration of simplified methods (a) elastic and (b) elastic–plastic.

$$\Delta\varepsilon_{11(m)} = \left[\frac{-\upsilon_m}{E_m} - \frac{1}{6}\left(\sum_{r=1}^{3} C_r \frac{1-\mathrm{e}^{-\alpha_r \Delta z}}{\alpha_r}\right)^{-1} \Delta z\right](\Delta\sigma_{22(m)} + \Delta\sigma_{33(m)}) + \frac{1}{2}\sum_{r=1}^{3}\left[\left(C_r \frac{1-\mathrm{e}^{-\alpha_r \Delta z}}{\alpha_r \Delta z}\right)^{-1} S_{11}^{(r)}(1-\mathrm{e}^{-\alpha_r \Delta z})\Delta z\right], \tag{4}$$

$$\Delta\varepsilon_{22(m)} = \left[\frac{1}{E_m} + \frac{1}{3}\left(\sum_{r=1}^{3} C_r \frac{1-\mathrm{e}^{-\alpha_r \Delta z}}{\alpha_r}\right)^{-1} \Delta z\right](\Delta\sigma_{22(m)}) - \left[\frac{-\upsilon_m}{E_m} - \frac{1}{6}\left(\sum_{r=1}^{3} C_r \frac{1-\mathrm{e}^{\alpha_r \Delta z}}{\alpha_r}\right)^{-1} \Delta z\right](\Delta\sigma_{33(m)}) + \frac{1}{2}\sum_{r=1}^{3}\left[\left(C_r \frac{1-\mathrm{e}^{\alpha_r \Delta z}}{\alpha_r}\right)^{-1} S_{22}^{(r)}(1-\mathrm{e}^{-\alpha_r \Delta z})\Delta z\right], \tag{5}$$

$$\Delta\varepsilon_{33(m)} = \left[\frac{1}{E_m} + \frac{1}{3}\left(\sum_{r=1}^{3} C_r \frac{1-\mathrm{e}^{\alpha_r \Delta z}}{\alpha_r}\right)^{-1} \Delta z\right](\Delta\sigma_{33(m)}) - \left[\frac{-\upsilon_m}{E_m} - \frac{1}{6}\left(\sum_{r=1}^{3} C_r \frac{1-\mathrm{e}^{\alpha_r \Delta z}}{\alpha_r}\right)^{-1} \Delta z\right](\Delta\sigma_{22(m)}) + \frac{1}{2}\sum_{r=1}^{3}\left[\left(C_r \frac{1-\mathrm{e}^{\alpha_r \Delta z}}{\alpha_r}\right)^{-1} S_{33}^{(r)}(1-\mathrm{e}^{-\alpha_r \Delta z})\Delta z\right], \tag{6}$$

and

$$\Delta\varepsilon_{23(m)} = \left[\frac{1+\upsilon_m}{E_m} + \frac{1}{2}\left(\sum_{r=1}^{3} C_r \frac{1-\mathrm{e}^{\alpha_r \Delta z}}{\alpha_r}\right)^{-1} \Delta z\right](\Delta\sigma_{23(m)}) + \frac{1}{2}\sum_{r=1}^{3}\left[\left(C_r \frac{1-\mathrm{e}^{\alpha_r \Delta z}}{\alpha_r}\right)^{-1} S_{23}^{(r)}(1-\mathrm{e}^{-\alpha_r \Delta z})\Delta z\right]. \tag{7}$$

The intrinsic time scale (z) can be obtained from (Owolabi and Singh, 2003b)

$$\left(\sum_{r=1}^{r} C_r \frac{(1-\mathrm{e}^{-\alpha_r \Delta z})}{\alpha_r}\right)^2 - \frac{1}{4}\left[(\Delta S_{ij(m)})_q + \sum_{r=1}^{r}(S^r_{ij(m)})_{q-1}(1-\mathrm{e}^{-\alpha_r \Delta z})\right] \times \left[(\Delta S_{ij(m)})_q + \sum_{r=1}^{r}(S^r_{ij(m)})_{q-1}(1-\mathrm{e}^{-\alpha_r \Delta z})\right] = 0. \tag{8}$$

Writing Eq. (8) fully on the notch tip elements, using three terms in the Dirichlet series, gives

$$\begin{aligned}
&\left[\sum_{r=1}^{3} C_r \frac{(1-\mathrm{e}^{-\alpha_r \Delta z})}{\alpha_r}\right]^2 - \frac{1}{4}\left[(\Delta S^{E/N(r)}_{11(m)})^2 + (\Delta S^{E/N(r)}_{22(m)})^2 (\Delta S^{E/N(r)}_{33(m)})^2 + 2(\Delta S^{E/N(r)}_{23(m)})^2\right] \\
&- \frac{1}{4}\left[(2(\Delta S^{E/N(r)}_{11(m)})(S^{E/N(r)}_{11(m)}(1-\mathrm{e}^{-\alpha_r \Delta z}))) + (2(\Delta S^{E/N(r)}_{22(m)})(S^{E/N(r)}_{22(m)}(1-\mathrm{e}^{-\alpha_r \Delta z})))\right. \\
&\left. + \left(2(\Delta S^{E/N(r)}_{33(m)})(S^{E/N(r)}_{33(m)}(1-\mathrm{e}^{-\alpha_r \Delta z}))\right) + (4(\Delta S^{E/N(r)}_{23(m)})(S^{E/N(r)}_{23(m)}(1-\mathrm{e}^{-\alpha_r \Delta z})))\right] \\
&- \frac{1}{4}\left[\left(\sum_{r=1}^{3} S^{E/N(r)}_{11(m)}(1-\mathrm{e}^{-\alpha_r \Delta z})\right)^2 + \left(\sum_{r=1}^{3} S^{E/N(r)}_{22(m)}(1-\mathrm{e}^{-\alpha_r \Delta z})\right)^2 + \left(\sum_{r=1}^{3} S^{E/N(r)}_{33(m)}(1-\mathrm{e}^{-\alpha_r \Delta z})\right)^2\right. \\
&\left. + 2\left(\sum_{r=1}^{3} S^{E/N(r)}_{23(m)}(1-\mathrm{e}^{-\alpha_r \Delta z})\right)^2\right] = 0.
\end{aligned} \tag{9}$$

Note that, in Owolabi and Singh (2003b), three times in the series expansion of the Dirichlet series have been found to accurately model the matrix cyclic stress–strain curve.

3. Non-linear energy-based relations

Eqs. (4)–(9) will provide some of the set of equations necessary to define the local parameters. Additional equations are obtained using two energy-based principles discussed below.

3.1. PMMCs incremental equivalent strain energy density (ESED)

For PMMC, here, it is proposed that as long as the notch tip plasticity is localized, parameters that define its behavior can be found by comparing it to the local behavior obtained in a geometrically identical elastic body subjected to the same external tractions (see Fig. 1). Specifically, it is proposed that for the composite system, the weighted contribution of each of the elastic–plastic strain–stress components of the composite to the increment in strain energy density at the notch tip is the same as the contribution of each stress–strain components to the increment in composite strain energy density at the notch tip when obtained from elastic analysis. The proposed hypothesis gives the following relations when expanded at the notch tip elements

$$\left(\sigma^e_{22}\Delta\varepsilon^e_{22} + \frac{1}{2}\Delta\sigma^e_{22}\Delta\varepsilon^e_{22}\right) - V_f\left(\sigma^e_{22(f)}\Delta\varepsilon^e_{22(f)} + \frac{1}{2}\Delta\sigma^e_{22(f)}\Delta\varepsilon^e_{22(f)}\right) - V_m\left(\sigma^E_{22(m)}\Delta\varepsilon^E_{22(m)} + \frac{1}{2}\Delta\sigma^E_{22(m)}\Delta\varepsilon^E_{22(m)}\right) = 0, \tag{10}$$

$$\left(\sigma^e_{33}\Delta\varepsilon^e_{33} + \frac{1}{2}\Delta\sigma^e_{33}\Delta\varepsilon^e_{33}\right) - V_f\left(\sigma^e_{33(f)}\Delta\varepsilon^e_{33(f)} + \frac{1}{2}\Delta\sigma^e_{33(f)}\Delta\varepsilon^e_{33(f)}\right) - V_m\left(\sigma^E_{33(m)}\Delta\varepsilon^E_{33(m)} + \frac{1}{2}\Delta\sigma^E_{33(m)}\Delta\varepsilon^E_{33(m)}\right) = 0, \tag{11}$$

and

$$\left(\sigma^e_{23}\Delta\varepsilon^e_{23}+\frac{1}{2}\Delta\sigma^e_{23}\Delta\varepsilon^e_{23}\right)-V_f\left(\sigma^e_{23(f)}\Delta\varepsilon^e_{23(f)}+\frac{1}{2}\Delta\sigma^e_{23(f)}\Delta\varepsilon^e_{23(f)}\right)-V_m(\sigma^E_{23(m)}\Delta\varepsilon^E_{23(m)}+\frac{1}{2}\Delta\sigma^E_{23(m)}\Delta\varepsilon^E_{23(m)})=0. \tag{12}$$

In Eqs. (10)–(12) "e" represents notch tip components that can be found from an elastic analysis, and "E" represents matrix elastic–plastic components as estimated by the incremental PMMC ESED method. Note that higher order terms render the set of equations nonlinear. The nonlinear terms are introduced to increase the accuracy of the model.

3.2. PMMCs incremental total strain energy density (Neuber's method)

For PMMCs, here, it is proposed that for the composite system, the weighted contribution of each of the elastic–plastic strain-s-tress components of the constituents to the increment in total energy density at the notch tip is the same as the contribution of each stress–strain components to the increment in composite total strain energy density at the notch tip when obtained from elastic analysis. The proposed hypothesis gives the following relations when expanded at the notch tip elements:

$$\begin{aligned}&(\sigma^e_{22}\Delta\varepsilon^e_{22}+\varepsilon^e_{22}\Delta\sigma^e_{22}+\Delta\sigma^e_{22}\Delta\varepsilon^e_{22})-V_f(\sigma^e_{22(f)}\Delta\varepsilon^e_{22(f)}+\varepsilon^e_{22(f)}\Delta\sigma^e_{22(f)}+\Delta\sigma^e_{22(f)}\Delta\varepsilon^e_{22(f)})\\&\quad-V_m(\sigma^N_{22(m)}\Delta\varepsilon^N_{22(m)}+\varepsilon^N_{22(m)}\Delta\sigma^N_{22(m)}+\Delta\sigma^N_{22(m)}\Delta\varepsilon^N_{22(m)})=0,\end{aligned} \tag{13}$$

$$\begin{aligned}&(\sigma^e_{33}\Delta\varepsilon^e_{33}+\varepsilon^e_{33}\Delta\sigma^e_{33}+\Delta\sigma^e_{33}\Delta\varepsilon^e_{33})-V_f(\sigma^e_{33(f)}\Delta\varepsilon^e_{33(f)}+\varepsilon^e_{33(f)}\Delta\sigma^e_{33(f)}+\Delta\sigma^e_{33(f)}\Delta\varepsilon^e_{33(f)})\\&\quad-V_m(\sigma^N_{33(m)}\Delta\varepsilon^N_{33(m)}+\varepsilon^N_{33(m)}\Delta\sigma^N_{33(m)}+\Delta\sigma^N_{33(m)}\Delta\varepsilon^N_{33(m)})=0,\end{aligned} \tag{14}$$

and

$$\begin{aligned}&(\sigma^e_{23}\Delta\varepsilon^e_{23}+\varepsilon^e_{23}\Delta\sigma^e_{23}+\Delta\sigma^e_{23}\Delta\varepsilon^e_{23})-V_f(\sigma^e_{23(f)}\Delta\varepsilon^e_{23(f)}+\varepsilon^e_{23(f)}\Delta\sigma^e_{23(f)}+\Delta\sigma^e_{23(f)}\Delta\varepsilon^e_{23(f)})\\&\quad-V_m(\sigma^N_{23(m)}\Delta\varepsilon^N_{23(m)}+\varepsilon^N_{23(m)}\Delta\sigma^N_{23(m)}+\Delta\sigma^N_{23(m)}\Delta\varepsilon^N_{23(m)})=0.\end{aligned} \tag{15}$$

In Eqs. (13)–(15), "N" represents matrix elastic–plastic components as estimated by the incremental Neuber's method.

Either the PMMCs incremental ESED nonlinear relations (Eqs. (10)–(12)) or the PMMCs incremental Neuber's nonlinear relations (Eqs. (13)–(15)) can be used in conjunction with the matrix elastic–plastic constitutive relations (Eqs. (4)–(7)) and the intrinsic time-stress relation (Eq. (9)) to define the relationships needed to solve for the increments in the matrix elastic–plastic local strain and stress tensors and the increment in the intrinsic time scale. Each set consists of eight relations with eight unknowns (i.e. four incremental matrix strain, three incremental matrix stress components, and the incremental intrinsic time scale). Newton–Raphson's numerical method for solving a system of nonlinear equations can be employed to solve for the eight unknowns for each increment in applied loads. However, using the eight equations may be CPU time consuming, especially under complex cyclic loading. Consequently, each set of equations was reduced to four nonlinear equations with four unknowns as follows.

3.3. Simplified PMMCs ESED energy ratio equations

Substituting Eqs. (5)–(7) into Eqs. (10)–(12) and re-arranging the resulting set of equations yield the following three relations:

$$V_m\left[\sigma_{22}^E\left(\frac{1}{E_m}+\frac{1}{3}\left(\sum_{r=1}^{3}C_r\frac{1-e^{\alpha_r\Delta z}}{\alpha_r}\right)^{-1}\Delta z\right)+\frac{1}{4}\sum_{r=1}^{3}\left(\left(C_r\frac{1-e^{\alpha_r\Delta z}}{\alpha_r}\right)^{-1}S_{22}^{E(r)}(1-e^{-\alpha_r\Delta z})\Delta z\right)\right]\Delta\sigma_{22(m)}^E$$
$$+V_m\sigma_{22}^E\left[\frac{-\upsilon_m}{E_m}-\frac{1}{6}\left(\sum_{r=1}^{3}C_r\frac{1-e^{\alpha_r\Delta z}}{\alpha_r}\right)^{-1}\Delta z\right]\Delta\sigma_{33(m)}^E+\frac{1}{2}V_m\left[\frac{-\upsilon_m}{E_m}-\frac{1}{6}\left(\sum_{r=1}^{3}C_r\frac{1-e^{\alpha_r\Delta z}}{\alpha_r}\right)^{-1}\Delta z\right]\Delta\sigma_{22(m)}^E\Delta\sigma_{33(m)}^E$$
$$+\frac{1}{2}V_m\left[\frac{1}{E_m}+\frac{1}{3}\left(\sum_{r=1}^{3}C_r\frac{1-e^{\alpha_r\Delta z}}{\alpha_r}\right)^{-1}\Delta z\right](\Delta\sigma_{22(m)}^E)^2+\frac{1}{2}V_m\sigma_{22}^E\left[\left(\sum_{r=1}^{3}C_r\frac{1-e^{\alpha_r\Delta z}}{\alpha_r}\right)^{-1}S_{22}^{E(r)}(1-e^{-\alpha_r\Delta z})\right]\Delta z$$
$$-\left[\left(\sigma_{22}^e\Delta\varepsilon_{22}^e+\frac{1}{2}\Delta\sigma_{22}^e\Delta\varepsilon_{22}^e\right)-V_f\left(\sigma_{22(f)}^e\Delta\varepsilon_{22(f)}^e+\frac{1}{2}\Delta\sigma_{22(f)}^e\Delta\varepsilon_{22(f)}^e\right)\right]=0, \tag{16}$$

$$V_m\left[\sigma_{23}^E\left(\frac{1+\upsilon_m}{E_m}+\frac{1}{2}\left(\sum_{r=1}^{3}C_r\frac{1-e^{\alpha_r\Delta z}}{\alpha_r}\right)^{-1}\Delta z\right)+\frac{1}{4}\sum_{r=1}^{3}\left(\left(C_r\frac{1-e^{\alpha_r\Delta z}}{\alpha_r}\right)^{-1}S_{23}^{E(r)}(1-e^{-\alpha_r\Delta z})\Delta z\right)\right]\Delta\sigma_{23(m)}^E$$
$$+\frac{1}{2}V_m\left[\frac{1+\upsilon_m}{E_m}+\frac{1}{2}\left(\sum_{r=1}^{3}C_r\frac{1-e^{\alpha_r\Delta z}}{\alpha_r}\right)^{-1}\Delta z\right](\Delta\sigma_{23(m)}^E)^2+\frac{1}{2}V_m\sigma_{23}^E\left[\sum_{r=1}^{3}\left(\left(C_r\frac{1-e^{\alpha_r\Delta z}}{\alpha_r}\right)^{-1}S_{23}^{E(r)}(1-e^{-\alpha_r\Delta z})\Delta z\right)\right]$$
$$-\left[\left(\sigma_{23}^e\Delta\varepsilon_{23}^e+\frac{1}{2}\Delta\sigma_{23}^e\Delta\varepsilon_{23}^e\right)-V_f\left(\sigma_{23(f)}^e\Delta\varepsilon_{23(f)}^e+\frac{1}{2}\Delta\sigma_{23(f)}^e\Delta\varepsilon_{23(f)}^e\right)\right]=0, \tag{17}$$

and

$$V_m\sigma_{33}^E\left[\frac{-\upsilon_m}{E_m}-\frac{1}{6}\left(\sum_{r=1}^{3}C_r\frac{1-e^{\alpha_r\Delta z}}{\alpha_r}\right)^{-1}\Delta z\right]\Delta\sigma_{22(m)}^E$$
$$+V_m\left[\sigma_{33}^E\left(\frac{1}{E_m}+\frac{1}{3}\left(\sum_{r=1}^{3}C_r\frac{1-e^{\alpha_r\Delta z}}{\alpha_r}\right)^{-1}\Delta z\right)+\frac{1}{4}\sum_{r=1}^{3}\left(\left(C_r\frac{1-e^{\alpha_r\Delta z}}{\alpha_r}\right)^{-1}S_{33}^{E(r)}(1-e^{-\alpha_r\Delta z})\Delta z\right)\right]\Delta\sigma_{33(m)}^E$$
$$+\frac{1}{2}V_m\left[\frac{-\upsilon_m}{E_m}-\frac{1}{6}\left(\sum_{r=1}^{3}C_r\frac{1-e^{\alpha_r\Delta z}}{\alpha_r}\right)^{-1}\Delta z\right]\Delta\sigma_{22(m)}^E\Delta\sigma_{33(m)}^E$$
$$+\frac{1}{2}V_m\left[\frac{1}{E_m}+\frac{1}{3}\left(\sum_{r=1}^{3}C_r\frac{1-e^{\alpha_r\Delta z}}{\alpha_r}\right)^{-1}\Delta z\right](\Delta\sigma_{33(m)}^E)^2$$
$$+\frac{1}{2}V_m\sigma_{33}^E\left[\left(\sum_{r=1}^{3}C_r\frac{1-e^{\alpha_r\Delta z}}{\alpha_r}\right)^{-1}S_{33}^{E(r)}(1-e^{-\alpha_r\Delta z})\right]\Delta z$$
$$-\left[\left(\sigma_{33}^e\Delta\varepsilon_{33}^e+\frac{1}{2}\Delta\sigma_{33}^e\Delta\varepsilon_{33}^e\right)-V_f\left(\sigma_{33(f)}^e\Delta\varepsilon_{33(f)}^e+\frac{1}{2}\Delta\sigma_{33(f)}^e\Delta\varepsilon_{33(f)}^e\right)\right]=0. \tag{18}$$

Eqs. (16)–(18) when used in conjunction with Eq. (9) provide the four equations that are sufficient to solve for the three unknown matrix local stresses and the intrinsic time scale. The increments in the matrix strain components are then obtained separately using Eqs. (4)–(7).

3.4. Simplified PMMCs Neuber energy ratio equations

Substituting Eqs. (5)–(7) into Eqs. (13)–(15) and re-arranging the resulting set of equations yield the following three relations:

$$V_m\left[\sigma_{22}^N\left(\frac{1}{E_m}+\frac{1}{3}\left(\sum_{r=1}^{3}C_r\frac{1-e^{\alpha_r\Delta z}}{\alpha_r}\right)^{-1}\Delta z\right)+\varepsilon_{22}^N+\frac{1}{2}\sum_{r=1}^{3}\left(\left(C_r\frac{1-e^{\alpha_r\Delta z}}{\alpha_r}\right)^{-1}S_{22}^{N(r)}(1-e^{-\alpha_r\Delta z})\Delta z\right)\right]\Delta\sigma_{22(m)}^N$$
$$+V_m\sigma_{22}^N\left[\frac{-\upsilon_m}{E_m}-\frac{1}{6}\left(\sum_{r=1}^{3}C_r\frac{1-e^{\alpha_r\Delta z}}{\alpha_r}\right)^{-1}\Delta z\right]\Delta\sigma_{33(m)}^N+V_m\left[\frac{-\upsilon_m}{E_m}-\frac{1}{6}\left(\sum_{r=1}^{3}C_r\frac{1-e^{\alpha_r\Delta z}}{\alpha_r}\right)^{-1}\Delta z\right]\Delta\sigma_{22(m)}^N\Delta\sigma_{33(m)}^N$$
$$+V_m\left[\frac{1}{E_m}+\frac{1}{3}\left(\sum_{r=1}^{3}C_r\frac{1-e^{\alpha_r\Delta z}}{\alpha_r}\right)^{-1}\Delta z\right](\Delta\sigma_{22(m)}^N)^2+\frac{1}{2}V_m\sigma_{22}^N\left[\left(\sum_{r=1}^{3}C_r\frac{1-e^{\alpha_r\Delta z}}{\alpha_r}\right)^{-1}S_{22}^{N(r)}(1-e^{-\alpha_r\Delta z})\right]\Delta z$$
$$-[(\sigma_{22}^e\Delta\varepsilon_{22}^e+\varepsilon_{22}^e\Delta\sigma_{22}^e+\Delta\sigma_{22}^e\Delta\varepsilon_{22}^e)-V_f(\sigma_{22(f)}^e\Delta\varepsilon_{22(f)}^e+\varepsilon_{22(f)}^e\Delta\sigma_{22(f)}^e+\Delta\sigma_{22(f)}^e\Delta\varepsilon_{22(f)}^e)]=0, \tag{19}$$

$$V_m\sigma_{33}^N\left[\frac{-\upsilon_m}{E_m}-\frac{1}{6}\left(\sum_{r=1}^{3}C_r\frac{1-e^{\alpha_r\Delta z}}{\alpha_r}\right)^{-1}\Delta z\right]\Delta\sigma_{22(m)}^N+V_m\left[\sigma_{33}^N\left(\frac{1}{E_m}+\frac{1}{3}\left(\sum_{r=1}^{3}C_r\frac{1-e^{\alpha_r\Delta z}}{\alpha_r}\right)^{-1}\Delta z\right)+\varepsilon_{33}^N\right.$$
$$\left.+\frac{1}{2}\sum_{r=1}^{3}\left(\left(C_r\frac{1-e^{\alpha_r\Delta z}}{\alpha_r}\right)^{-1}S_{33}^{N(r)}(1-e^{-\alpha_r\Delta z})\Delta z\right)\right]\Delta\sigma_{33(m)}^N$$
$$+V_m\left[\frac{-\upsilon_m}{E_m}-\frac{1}{6}\left(\sum_{r=1}^{3}C_r\frac{1-e^{\alpha_r\Delta z}}{\alpha_r}\right)^{-1}\Delta z\right]\Delta\sigma_{22(m)}^N\Delta\sigma_{33(m)}^N$$
$$+V_m\left[\frac{1}{E_m}+\frac{1}{3}\left(\sum_{r=1}^{3}C_r\frac{1-e^{\alpha_r\Delta z}}{\alpha_r}\right)^{-1}\Delta z\right](\Delta\sigma_{33(m)}^N)^2+\frac{1}{2}V_m\sigma_{33}^N\left[\left(\sum_{r=1}^{3}C_r\frac{1-e^{\alpha_r\Delta z}}{\alpha_r}\right)^{-1}S_{33}^{N(r)}(1-e^{-\alpha_r\Delta z})\right]\Delta z$$
$$-[(\sigma_{33}^e\Delta\varepsilon_{33}^e+\varepsilon_{33}^e\Delta\sigma_{33}^e+\Delta\sigma_{33}^e\Delta\varepsilon_{33}^e)$$
$$-V_f(\sigma_{33(f)}^e\Delta\varepsilon_{33(f)}^e+\varepsilon_{33(f)}^e\Delta\sigma_{33(f)}^e+\Delta\sigma_{33(f)}^e\Delta\varepsilon_{33(f)}^e)]=0, \tag{20}$$

and

$$V_m\left[\sigma_{23}^N\left(\frac{1+\upsilon_m}{E_m}+\frac{1}{2}\left(\sum_{r=1}^{3}C_r\frac{1-e^{\alpha_r\Delta z}}{\alpha_r}\right)^{-1}\Delta z\right)+\varepsilon_{23}^N+\frac{1}{2}\sum_{r=1}^{3}\left(\left(C_r\frac{1-e^{\alpha_r\Delta z}}{\alpha_r}\right)^{-1}S_{23}^{N(r)}(1-e^{-\alpha_r\Delta z})\Delta z\right)\right]\Delta\sigma_{23(m)}^N$$
$$+V_m\left[\frac{1+\upsilon_m}{E_m}+\frac{1}{2}\left(\sum_{r=1}^{3}C_r\frac{1-e^{\alpha_r\Delta z}}{\alpha_r}\right)^{-1}\Delta z\right](\Delta\sigma_{23(m)}^N)^2+\frac{1}{2}V_m\sigma_{23}^N\left[\sum_{r=1}^{3}\left(\left(C_r\frac{1-e^{\alpha_r\Delta z}}{\alpha_r}\right)^{-1}S_{23}^{N(r)}(1-e^{-\alpha_r\Delta z})\Delta z\right)\right]$$
$$-[(\sigma_{23}^e\Delta\varepsilon_{23}^e+\varepsilon_{23}^e\Delta\sigma_{23}^e+\Delta\sigma_{23}^e\Delta\varepsilon_{23}^e)-V_f(\sigma_{23(f)}^e\Delta\varepsilon_{23(f)}^e+\varepsilon_{23(f)}^e\Delta\sigma_{23(f)}^e+\Delta\sigma_{23(f)}^e\Delta\varepsilon_{23(f)}^e)]=0. \tag{21}$$

Eqs. (19)–(21), when used in conjunction with Eq. (9), provide the four equations that are sufficient to solve for the three unknown matrix local stresses and the intrinsic time scale. The increments in the matrix strain components are then obtained separately using Eqs. (4)–(7). The resulting two sets of nonlinear equations are given by Eqs. (9), (16)–(18) and Eqs. (9), (19)–(21) for the PMMCs ESED and the PMMCs Neuber methods, respectively. Each set can be solved using the Newton–Raphson's numerical method for solving systems of nonlinear relations.

4. Numerical procedure

In this section, the numerical procedure for evaluating the two sets of nonlinear relations is given. The scheme, illustrated in a pseudo-code shown in Fig. 2, is the same for both models. The scheme calculates the

Note: All parameters and variables are as defined in the main text.
Initialize: The composite stress (σ_{ij}) and strain (ε_{ij}) tensors; the reinforcement stress ($\sigma_{ij(f)}$) and strain ($\varepsilon_{ij(f)}$) tensors; and the matrix stress ($\sigma^{N/E}_{ij(m)}$) and strain ($\varepsilon^{N/E}_{ij(m)}$) tensors.

Input:
V_f = volume fraction of reinforcement, V_m = volume fraction of matrix
C_r, α_r = material constants
L = number of load steps in the load path, q = number of load increments

1 Do L times
2 Read composite elastic history (ε^e_{ij} and σ^e_{ij})),
2.1 For N = 1 to q
2.1.1 Compute the increment in the composite elastic history (i.e. $\Delta\varepsilon^e_{ij} = \varepsilon^e_{ij}/q$ and $\Delta\sigma^e_{ij} = \sigma^e_{ij}/q$)
2.1.2 Compute ($\Delta\varepsilon^e_{ij(f)}$) and ($\Delta\sigma^e_{ij(f)}$) from $\Delta\sigma^e_{ij}$ (Owolabi and Singh, 2005)
2.1.3 Compute ($\Delta\varepsilon^e_{ij(m)}$) and ($\Delta\sigma^e_{ij(m)}$) from $\Delta\sigma^e_{ij}$ (Owolabi and Singh, 2005)
2.1.4 Use the linear solutions as initial guesses
2.1.5 Use the current solutions as initial guesses in the Newton-Ralphson non-linear solver to compute (Δz), ($\Delta\varepsilon^{N/E}_{ij(m)}$) and ($\Delta\sigma^{N/E}_{ij(m)}$). (Eqs. (9), (16)-(18) or Eqs (9), (19)-(21) and Eqs. (4) -(7))
2.1.6 If ($\|F(A(q)\|$ & $\| dA(q) \| \leq 10^{-8}$)
Compute ($\Delta\varepsilon_{ij}$) and ($\Delta\sigma_{ij}$) using $\Delta\varepsilon^{N/E}_{ij(m)}$, $\Delta\sigma^{N/E}_{ij(m)}$, $\Delta\varepsilon^e_{ij(f)}$, ($\Delta\sigma^e_{ij(f)}$)
Update ε_{ij} and σ_{ij}
Update S^r, Eq. (3)
Else
Go to 2.1.6
End If
2.1.7 End For
3 Output

Fig. 2. Pseudo-code for notch root elastic–plastic strain–stress analysis for PMMCs.

composite elastic–plastic strain and stress histories at a geometric discontinuity given the material constants and the elastic local strain–stress histories obtained from the elastic solutions. The composite local elastic–plastic strain and stress histories that result in response to a cyclically applied load are evaluated incrementally. That is, they are evaluated for each small increment in the applied load. The elastic–plastic constitutive relations are applicable from the onset of loading.

For each increment of external load, the increments in the matrix local stress and the intrinsic time scale are obtained using the two sets of nonlinear equations given by Eqs. (9), (16)–(18) and Eqs. (9), (19)–(21) for the PMMCs ESED and the PMMCs Neuber methods, respectively. As stated earlier, since the equations are nonlinear, a numerical iterative method such as Newton–Raphson method is required to obtain the unknowns. The linear solutions for the increments in the matrix stress components and the increment in the intrinsic time scale are used as initial guesses for the unknowns in the Newton–Raphson routine. This reduces the computational time required to obtain the unknowns since the linear solutions provide a close approximation to the nonlinear solutions. It also ensures that the systems of equations converge. To obtain the linear solutions for the matrix stress–strain increments, the intrinsic time scale is first obtained from the nonlinear equation, Eq. (9), using an iterative numerical Secant method. The increment in the time scale is

then substituted into the linear forms of each set of seven equations (i.e. Eqs. (4)–(7), (10)–(12), and Eqs. (4)–(7), (13)–(15) for the PMMCs ESED and the PMMCs Neuber method, respectively). These linear forms are obtained by ignoring the nonlinear terms (i.e. terms with higher orders) in the solution sets. The resulting linear sets of algebraic equations are then solved simultaneously to obtain the linear solutions of the increments in the matrix stress and strain tensors. Using these linear solutions of the matrix stress and the intrinsic time scale obtained as initial guesses, the two set of nonlinear equations given by Eqs. (9), (16)–(18) and Eqs. (9), (19)–(21) for the PMMCs ESED and the PMMCs Neuber methods, respectively, are then solved for the unknown increments in the intrinsic time and matrix stress tensor using Newton–Raphson method. The increment in the matrix strain tensor is then obtained separately using Eqs. (4)–(7). The final state of stress and strain at a point can then be obtained by adding the increments to the previous stress–strain history. The increments in the reinforcement stress and strain can be obtained from the elastic analysis and the elastic stress concentration factors (Owolabi and Singh, 2005). For each point in the loading history the composite local elastic–plastic strain and stress tensors can be obtained using the elastic–plastic matrix strains and stresses, the elastic reinforcement strains and stresses, and the work relation (Owolabi and Singh, 2003b).

It is important to discuss briefly the convergence criteria used to determine when the Newton–Raphson solution has converged. Since we are determining the solution of a system of nonlinear equations, it is reasonable to assume that the solution converges when the norm of the matrix containing the set of solutions is very small on substituting the solutions provided at each iteration step (i.e. $\|F(A(q))\|$ is small, where F is the matrix of the function, and $A(q)$ is the matrix of the solution of F at an iteration step q). In the implementation of the scheme, the norm was made less than or equal to 10^{-8}. In addition, it is required that the solution at an iteration step is close to the solution as the number of iteration tends to infinity (i.e. $A(q) = A(\infty)$). In other words, it is reasonable to require that $\|\mathrm{d}A(q)\|$ be small, where $\mathrm{d}A(q)$ is the difference between two successive iterations. Both requirements were used as convergence criteria in this research. This norm was also made less than or equal to the order of 10^{-8}.

5. Results and discussions

The numerical scheme presented in Section 4 is used to implement the analytical models discussed in Section 3. The numerical results are compared with the results obtained from experimental tests conducted using specimens machined from 6061/Al_2O_3/xxp-T6 PMMC with 10 and 20% volume fractions of reinforcing particles. The specimens with geometries shown in Fig. 3 were subjected to cyclic tension (P)–torsion (T) load paths shown in Figs. 4 and 5. In the figures, the loading sequence is indicated by numbers and arrows (note that the loading sequence starts and ends at 0). 3D image correlation technology (Aramis

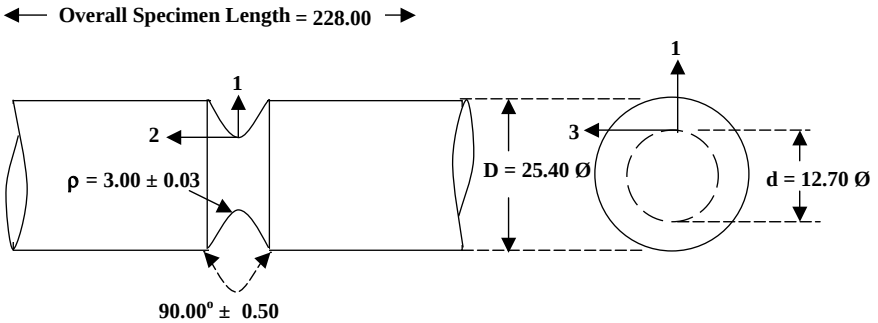

Fig. 3. Geometry of the notched specimen (all dimensions in mm).

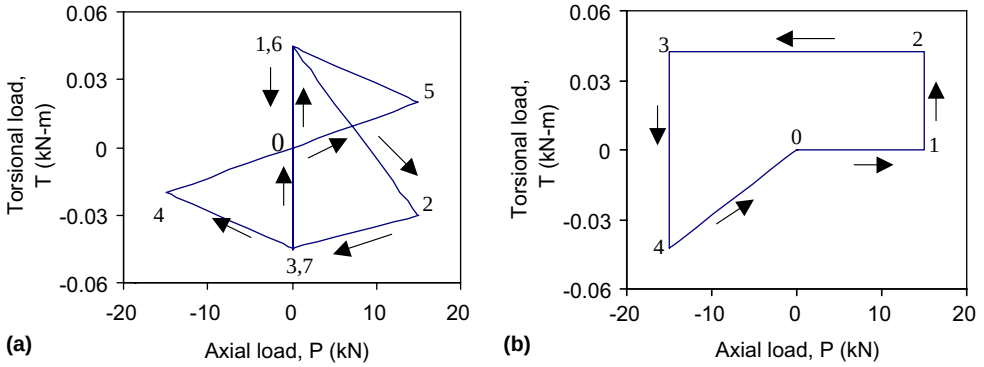

Fig. 4. Variable amplitudes non-proportional loading (a) path 1 and (b) path 2.

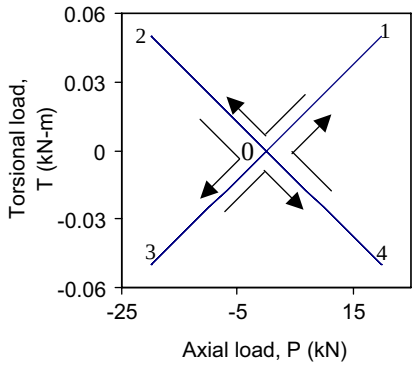

Fig. 5. X-shape balanced loading with equal frequencies in torsion and tension.

Users Manual, 2003) was used to obtain the experimental strains. The results of the experimental tests and the numerical predictions are presented as plots of local elastic–plastic shear strain, ε_{23}, against axial strain, ε_{22}, for all load paths tested as shown in Figs. 6–11. The figures show the experimental and calculated results for both the 10% and 20% volume fraction of reinforcing particles. The results were given on different plots for clarity purpose.

The results of experimental strain measurements and the results of the simplified models for the variable amplitude loading paths shown in Fig. 4 are presented in Figs. 6(a–c), 7(a–c), 8(a–c), 9(a–c). The simplified models predict the general trends observed in the experimental results for the load paths and volume fractions considered. That is, the models predicted regions of elastic unloading at each corner of the loading path, followed by regions of elastic–plastic behavior to the next corner. The results of the load paths indicate that the methodologies are capable of predicting the elastic–plastic local strains for these variable amplitude load sequences. Although the results for both volume fractions of reinforcement indicate that the analytical methodologies sometimes over-predict, and at other points under-predict the notch root elastic–plastic strains, the differences are small in all cases. These differences may be due to the inability of the incremental mean field theory to incorporate the point-to-point stress and strain fields in the composite and its constituents. The differences between the experimental and the predicted results could also have been due to the approximate values of the material constants used in the endochronic theory-based constitutive model.

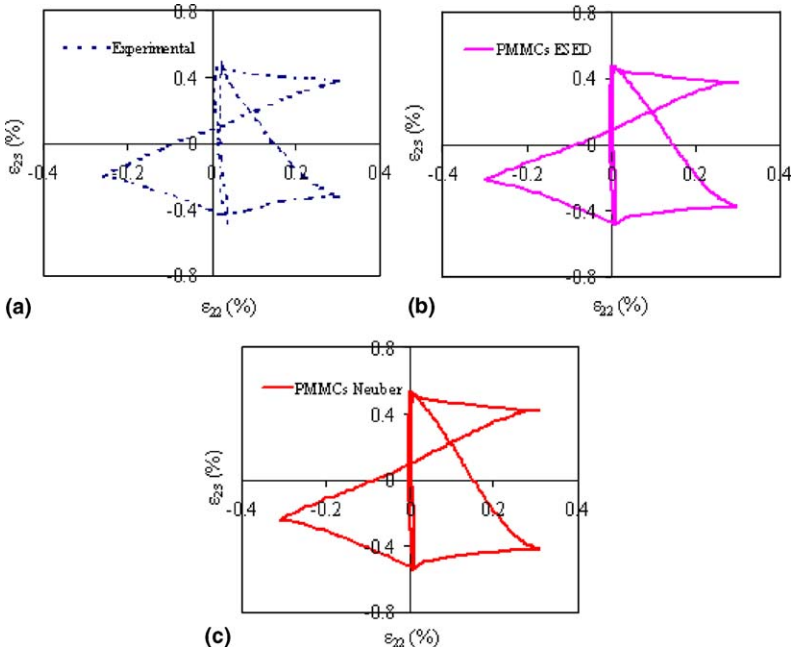

Fig. 6. Notch root shear strains versus axial strains for variable amplitude load path in Fig. 4(a), 10% volume fraction (a) experimental (b) PMMCs ESED and (c) PMMCs Neuber.

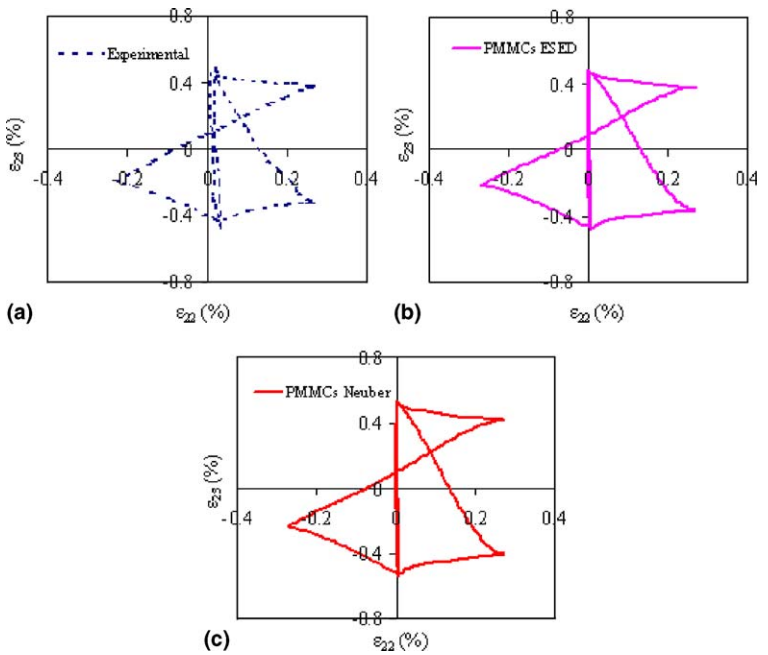

Fig. 7. Notch root shear strains versus axial strains for variable amplitude load path in Fig. 4(a), 20% volume fraction (a) experimental (b) PMMCs ESED, and (c) PMMCs Neuber.

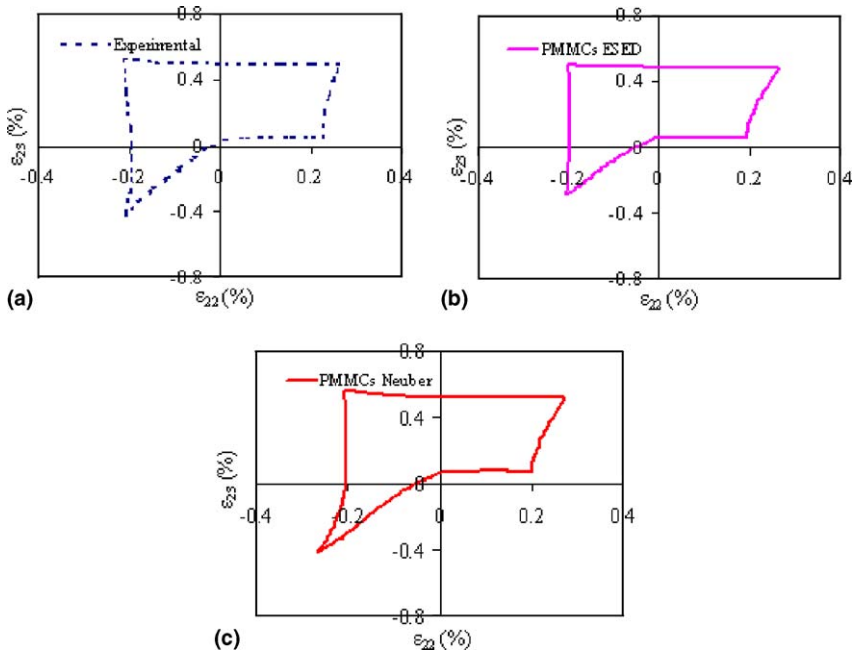

Fig. 8. Notch root shear strains versus axial strains for variable amplitude load path in Fig. 4(b), 10% volume fraction (a) experimental (b) PMMCs ESED, and (c) PMMCs Neuber.

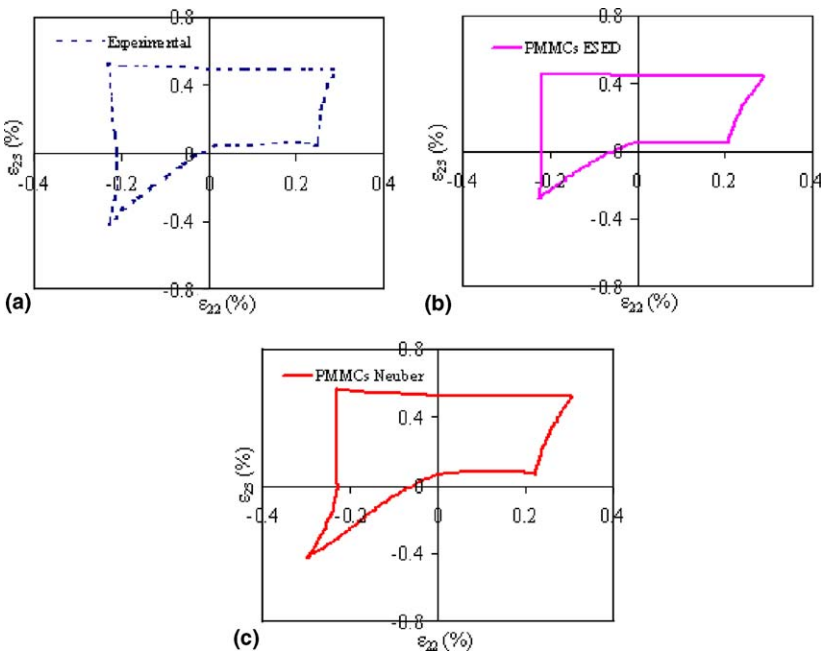

Fig. 9. Notch root shear strains versus axial strains for variable amplitude load path in Fig. 4(b), 20% volume fraction (a) experimental (b) PMMCs ESED, and (c) PMMCs Neuber.

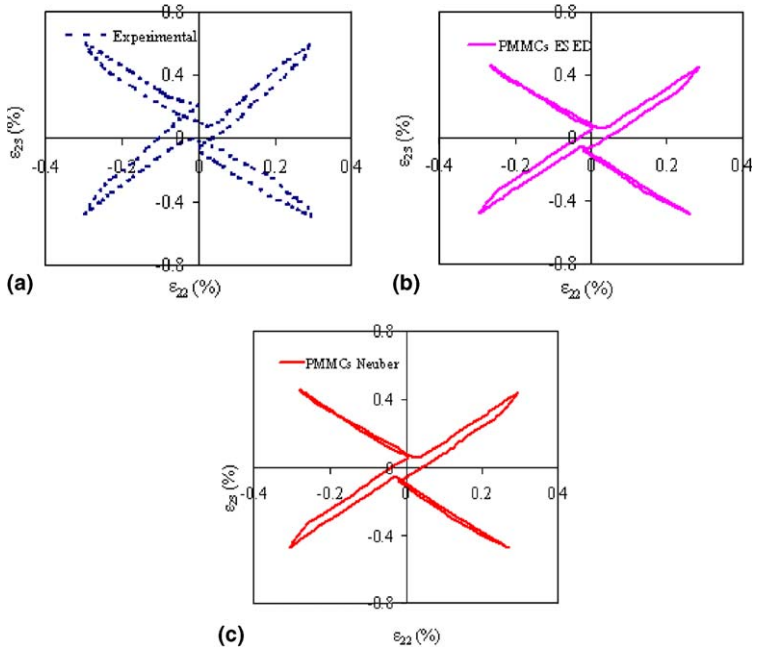

Fig. 10. Notch root shear strains versus axial strains for load path in Fig. 5, 10% volume fraction (a) experimental (b) PMMCs ESED, and (c) PMMCs Neuber.

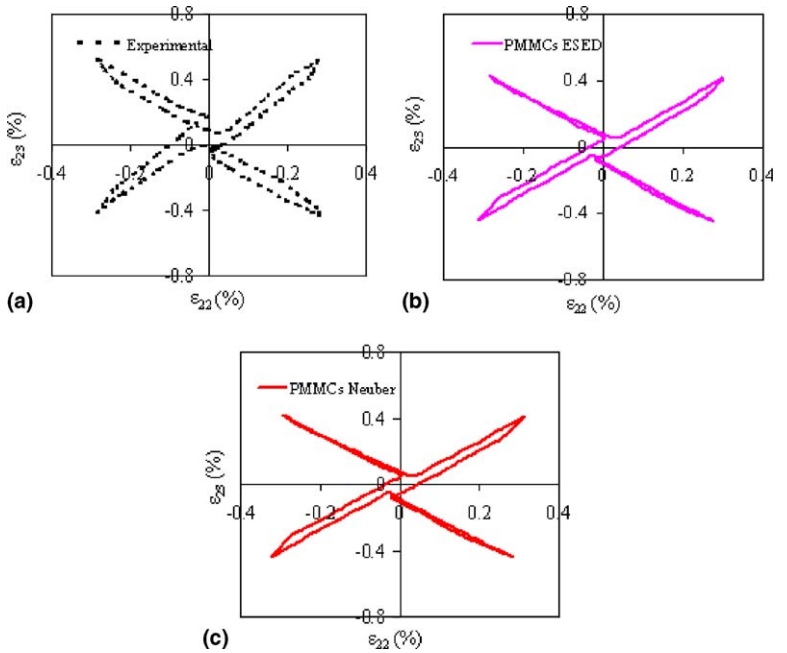

Fig. 11. Notch root shear strains versus axial strains for load path in Fig. 5, 20% volume fraction (a) experimental (b) PMMCs ESED, and (c) PMMCs Neuber.

Figs. 10(a–c) and 11(a–c) show the experimental and predicted results for the X-shape loading path (Fig. 5). In the X-path, the segments are linear between zero and maximum. The cyclic load was applied in a counter-clockwise direction. The models results are in good agreement with experimental results.

It is important to state that the analytical methodologies predict the local strains in the specimens with both volume fractions of reinforcements. This clearly shows that the models respect the heterogeneous nature of the material. The difference in the strain results for the 10% and 20% volume fractions may be attributed to the differences in the amplitude of the applied loads and the effects of volume fractions on the matrix plastic strains. In the assessment of the constitutive models in Owolabi and Singh (2003b), the results obtained show that the PMMC materials become stiffer with increasing volume fraction of reinforcement, thus, leading to diminishing plastic strains. This heterogeneous nature of the material has been incorporated into the models by accounting for the interactions in the stress fields between the particles in the incremental mean field theory used, and also by incorporating the localized deformation of both the matrix and the reinforcing particles into the proposed simplified models developed.

6. Conclusions

In this paper, two sets of nonlinear energy-based equations have been implemented to predict the composite elastic–plastic local strains for a two-phase composite system subjected to variable amplitude loads. The numerical results compare very well to the experimental results for the geometry and load paths tested. The results further indicate the ability of the models to account for the heterogeneous nature of particulate metal matrix composites since the analytical methodologies predict the local strains in the materials for both volume fraction of reinforcement.

Acknowledgements

The authors greatly acknowledged the financial support given by the University of Manitoba in form of Graduate Fellowship, Faculty of Engineering in form of Graduate Awards, and the research grants provided by National Science and Engineering Research Council of Canada (NSERC) and Canadian Foundation for Innovation (CFI).

References

Aramis Users Manual, version 5, GOM Measurements, Braunschweig, Germany, 2003.

Barkey, M.E., 1993. Calculation of notch strains under multiaxial nominal loading. Ph.D. Thesis, University of Illinois at Urbana, Champagne.

Barkey, M.E., Socie, D.F., Hsai, K.J., 1994. A yield surface approach to the estimation of notch strains for proportional and non-proportional cyclic loading. Journal of Engineering Materials and Technology 116, 173–179.

Gu, R.J., Lee, Y., 1997. A new method for estimating non-proportional notch root stresses and strains. Journal of Engineering Materials and Technology 119, 40–45.

Hsu, S.Y., Jain, S.K., Griffin Jr., O.J., 1991. Verification of endochronic theory for non-proportional loading paths. Journal of Engineering Mechanics 117, 110–131.

Lee, Y., Chiang, Y., Wong, H., 1995. A constitutive model for estimating notch strains. Journal of Engineering Materials and Technology 117, 33–40.

Li, Y.Y., Chen, Y., 1990. An incremental plastic analysis of multiphase materials. Journal of Applied Mechanics 57, 562–5614.

Owolabi, G.M., Singh, M.N.K., 2003a. Elastic–plastic behavior of notched PMMCs under multiaxial loading. In: Proceeding of the 19th Canadian Congress of Applied Mechanics, University of Calgary, Calgary, AB. vol. 1, pp. 132–133.

Owolabi, G.M., Singh, M.N.K., 2003b. A comparison between two models that predict the elastic–plastic behavior of particulate metal matrix composites under multiaxial fatigue type loading. In: Proceedings of the 2003 International Mechanical Engineering Congress and Exposition, November 16–21, Washington DC, USA. 10 p.

Owolabi, G.M., Singh, M.N.K., 2005. Notch-root elastic–plastic strain–stress in particulate metal matrix composites subjected to general loading conditions. Journal of ASTM International 2 (6).

Singh, M.N.K., Glinka, G., Dubey, R.N., 1996. Elastic–plastic stress–strain calculation in notched bodies subjected to non-proportional loading. International Journal of Fracture, 39–60.

Valanis, K.C., 1980. Fundamental consequences of a new intrinsic time measure: plasticity as a limit of the endochronic theory. Archives of Mechanics 32, 171–191.